Original Article

Biomimetic cytomembrane-coated ZIF-8-loaded DMDD nanoparticle and sonodynamic co-therapy for cancer

Shuqi Zhao[1#], Meifeng Chen[1#], Zhu Yu[2], Thi Thai Hoa Pham[3], Shutian Mo[1], Yongfei He[1], Tianyi Liang[1], Wenlong Cao[2], Chuangye Han[1,4]

[1]Department of Hepatobiliary Surgery, The First Affiliated Hospital of Guangxi Medical University, Nanning, China; [2]Department of Gastrointestinal Surgery, The First Affiliated Hospital of Guangxi Medical University, Nanning, China; [3]Zhuang & Yao Medicine Research and Development Center, Guangxi International Zhuang Medicine Hospital, Nanning, China; [4]Guangxi Key Laboratory of Enhanced Recovery after Surgery for Gastrointestinal Cancer, Nanning, China

Contributions: (I) Conception and design: C Han, W Cao; (II) Administrative support: C Han, W Cao; (III) Provision of study materials or patients: S Zhao, M Chen; (IV) Collection and assembly of data: Z Yu; (V) Data analysis and interpretation: Y He, S Mo, T Liang; (VI) Manuscript writing: All authors; (VII) Final approval of manuscript: All authors.

[#]These authors contributed equally to this work.

Correspondence to: Chuangye Han. Department of Hepatobiliary Surgery, The First Affiliated Hospital of Guangxi Medical University, Nanning, China. Email: hanchuangye@hotmail.com. Wenlong Cao. Department of Gastrointestinal Surgery, The First Affiliated Hospital of Guangxi Medical University, Nanning, China. Email: 47189015@qq.com.

Background: Breast cancer (BC) is the most common type of cancer affecting females. It is also a leading cause of cancer-related death in women worldwide.

Methods: Sonodynamic therapy (SDT) is an emerging therapeutic strategy for cancer treatment. SDT ensures non-invasive penetration of deep tumors and results in activation of non-toxic sonosensitizers administered in deep tumor sites to become cytotoxic. It has been reported that 2-dodecyl-6-methoxycyclohexa-2,5-diene-1,4-dione (DMDD) has a significant anti-tumor effect against various cancer types including BC. However, DMDD is hydrophobic. Therefore, a one-step encapsulation method was used in the current study to construct zeolitic imidazole frameworks-8 (ZIF-8) loaded with DMDD and sonosensitizer chlorin e6 (Ce6). ZIF-8 was further modified by coating it with a biomimetic cell membrane to improve targeted delivery.

Results: *In vitro* and *in vivo* results indicated that the nanomedicines had great biocompatibility properties and targeting ability. The nanocomposite exhibited a higher release rate under an acidic tumor microenvironment. The tumor killing effect of reactive oxygen species (ROS) generated from Ce6 and inhibition of tumor growth was enhanced after ultrasound (US) treatment, which might be caused by the increase in apoptosis rate.

Conclusions: These findings show that the combination of nanomedicine and SDT provides a potential therapeutic method for BC.

Keywords: Breast cancer (BC); 2-dodecyl-6-methoxycyclohexa-2,5-diene-1,4-dione (DMDD); metal-organic framework; sonodynamic therapy; ZIF-8 nanoparticles

Submitted Jul 06, 2022. Accepted for publication Aug 17, 2022.
doi: 10.21037/atm-22-3646
View this article at: https://dx.doi.org/10.21037/atm-22-3646

Introduction

Breast cancer (BC) is the most common female malignant tumor and a leading cause of cancer-related death in women worldwide (1,2). Although the incidence of BC has reduced in recent years, the 5-year survival rate of BC patients diagnosed at advanced stages is approximately 26%

(3,4). The main therapeutic approaches for BC include surgery, chemotherapy, radiotherapy, hormonal therapy, and molecular-targeted therapy (4). Although significant advances in clinical treatments and diagnosis have been achieved in the recent past, drug resistance and a high recurrence rate lower the survival of BC patients (5).

Chinese medicine monomer components have been widely studied for their anti-tumor effects. Oroxylin A is a flavonoid isolated from Scutellariae radix, which was shown to inhibit the proliferation and epithelial-mesenchymal transition of BC cells (6). Procyanidin A1 is a member of the procyanidin family which exhibits anti-inflammatory and antioxidant effects (7). Averrhoa carambola L. is a Chinese herbal medicine from which 2-dodecyl-6-methoxycyclohexa-2,5-diene-1,4-dione (DMDD) can be extracted. Previous studies reported that DMDD exhibited anti-tumor effects against BC in mice (8-11). In addition, DMDD can block tumorigenesis through modulation of the cell cycle in lung cancer (12). However, DMDD has poor solubility in water, thus limiting its application as an anti-tumor agent.

Sonodynamic therapy (SDT) is an emerging therapeutic method for cancer treatment. Compared to photo-inspired therapy and traditional monotherapy, SDT provides many opportunities and benefits, including deeper tissue penetration, high precision, less side effects, and good patient compliance (13). SDT involves the combination of ultrasound (US) and sonosensitizers. The relatively non-toxic chemical agents (sonosensitizers) are administered to cells, resulting in simultaneous or subsequent sensitivity to US irradiation (14). Sensitization and US irradiation do not have tumoricidal effects on their own. However, low-intensity US activates non-toxic sonosensitizers making them cytotoxic through the generation of reactive oxygen species (ROS), thus killing cells (14-16). US can penetrate deep tumors, thereby activating sonosensitizers administered in deep tumor sites. This property provides the possibility for effective therapy for deep solid tumors, and has been widely explored in different cancers, such as pancreatic and liver cancer (15,17,18).

The type of sonosensitizer determines the efficacy of SDT, as the physicochemical properties can influence the therapeutic effect, and the type determines the safety of drug residues in the body (19,20). Chlorin e6 (Ce6) is a porphyrin with low side effects. It is an organic sonosensitizer that can accumulate in tumor sites and is activated by light and US (21-23). However, Ce6 is a hydrophobic compound and is cleared rapidly in long-term blood circulation, thus reducing its efficacy (24,25). In the current study, DMDD and Ce6 were loaded onto a metal framework, zeolitic imidazole frameworks-8 (ZIF-8), to improve targeted delivery of the sonosensitizer and DMDD. ZIF-8 is a representative metal-organic framework (MOF), comprising of Zn^{2+} and 2-methylimidazolate ligands (26). It is characterized by excellent chemical and thermal stability, high surface area, and abundant micropores, making it an excellent framework for the loading of drugs (27,28). Notably, ZIF-8 is pH responsive, thus it degrades under an acidic environment while exhibiting high stability under neutral conditions. This indicates that ZIF-8 can be used to deliver drugs and ensure targeted release in the acidic tumor microenvironment (29-31). These properties improve the local drug concentration at tumor sites and strengthen the anti-tumor effect.

Therefore, a ZIF-8 framework was constructed for loading sonosensitizers Ce6 and DMDD to achieve targeted delivery and release of the compounds in the tumor site, and the co-operation of SDT and DMDD improved the anti-tumor effects of nanoparticles (*Figure 1*). We present the following article in accordance with the ARRIVE reporting checklist (available at https://atm.amegroups.com/article/view/10.21037/atm-22-3646/rc).

Methods

Characterization of nanoparticles

The surface potential and size of nanomedicines were determined using ZS90 Zeta Sizer (Malvern, UK). Morphological and structural characterization of ZDC@M nanocomposites was performed using scanning electron microscopy (SEM, SU8020, Japan) and transmission electron microscopy (TEM, JEM-2100F, US). The ultrasonic source was supplied by the WED-100 ultrasonic treatment machine (Welld, China). A FACSVerse flow cytometer (BD, USA) was used for the determination of the cell apoptosis rate and rate of nanoparticle uptake. Nanoparticle uptake and intracellular hypoxia were observed under a laser confocal scanning microscope (LCSM) (Leica, Germany).

DMDD extraction

The root of Averrhoa carambola L. was a classification of Oxalidaceae plant. Dried roots were milled to obtain a coarse powder. The processes to extract, isolate, and

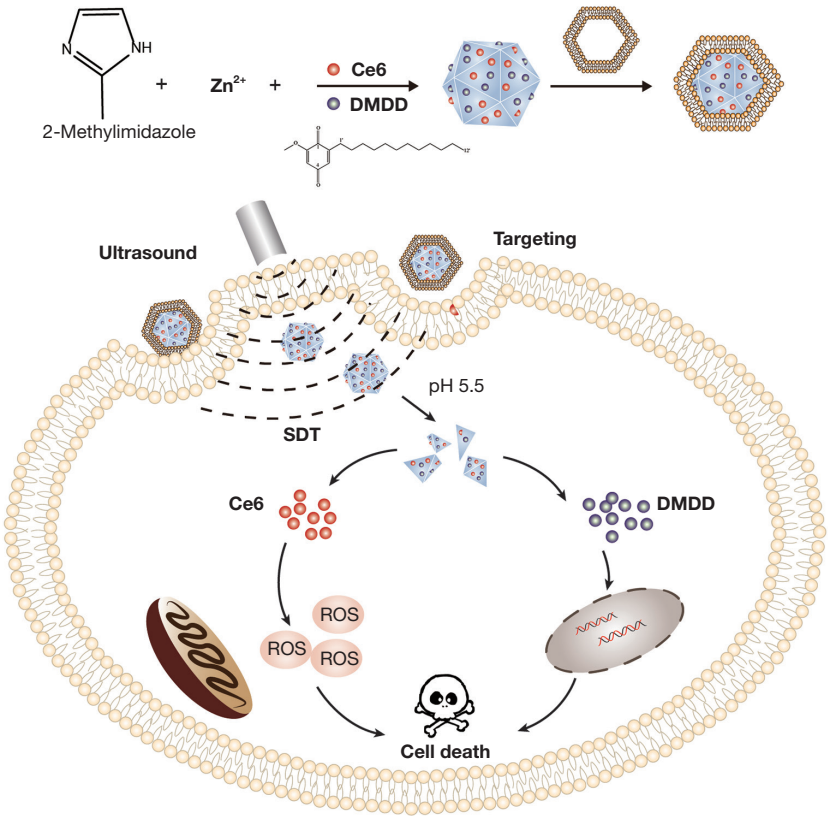

Figure 1 Schematic illustration of the synthesis process of the ZDC@M nanoparticles and pH-sensitive ultrasound triggered SDT combined with DMDD therapy. ZDC@M, ZIF-8@ DMDD/Ce6@ cytomembrane; ZIF-8, zeolitic imidazole frameworks-8; SDT, sonodynamic therapy; DMDD, 2-dodecyl-6-methoxycyclohexa-2,5-diene-1,4-dione.

identify DMDD were conducted following methods described previously (32,33). The purity of DMDD was approximately 95%. After dissolving in dimethyl sulfoxide (DMSO, Solarbio, China), DMDD (10 mM) was prepared for use in subsequent experiments.

Synthesis of ZIF-8@ DMDD/Ce6 (ZDC)

We use one-pot method to construct drugs/ZIF-8 materials. In the growth process of ZIF-8, the drug is loaded into ZIF-8. A total of 0.3 g $Zn(NO_3)_2{\cdot}6H_2O$ (Aladdin, China) and 0.17 g 1,2-dimethylimidazole (1,2-MIL, Aladdin, China) were separately dissolved in 40 mL methanol. The 1,2-MIL solution was added into the $Zn(NO_3)_2{\cdot}6H_2O$ solution. After stirring for 2 min, DMDD and 1 mg of Ce6 (Frontier Scientific, US) were separately added into the mixture and stirred for another 5 min. The mixture was allowed to stand for 4 h then washed sequentially with methanol and DMSO twice and centrifuged at 12,000 rpm for 10 min. The sediment of ZDC was obtained and freeze dried.

According to the same procedures, ZIF-8@Ce6 (ZC) and ZIF-8@DMDD (ZD) were synthesized. Finally, the loading efficiency was calculated using the Eq. [1] in the Appendix 1.

Synthesis of ZIF-8@ DMDD/Ce6 @cytomembrane (ZDC@M)

The cytomembrane of 4T1 cells was extracted by the Mem-PER™ Plus Protein Extraction Kit (Thermo Fisher Scientific, USA). Then, 2 mg/mL of ZDC (1 mL) was mixed with 4 mg/mL of cytomembrane fragments of 4T1 cells (1 mL) and oscillated for 2 h at 4 ℃. A liposome extruder was used to repeatedly extrude the aforementioned mixture. The mixture was then centrifuged for 10 min (4 ℃, 12,000 g), the sediment was obtained, and this comprised the ZDC@M.

Gel electrophoresis

Gel electrophoresis was used to verify that the nanomedicine was coated by cytomembrane. Different protein samples with the same concentration were loaded onto 10% SDS-PAGE (sodium dodecyl sulfate-polyacrylamide gels) for separation. The gel was then stained with Coomassie Blue (Beyotime, China) for 2 h and washed thoroughly with water for 6 h. The gel was observed under a microscope using ECL western blotting substrate and images were obtained.

Hemolysis assay

A hemolysis assay was conducted for the evaluation of the blood compatibility of ZDC@M nanomedicine. Fresh blood samples were acquired from nude mice. After washing thrice with PBS (phosphate buffer solution), red blood cells (RBCs) were collected. RBC solution (200 μL) was mixed with 800 μL PBS and different concentrations of nanomedicines were added. PBS and pure water were defined as NC (negative control) and PC (positive control), respectively. Each group had 3 replicates. After being incubated at 37 ℃ for 4 h, these RBC solutions were then centrifuged (3,500 rpm, 5 min) and the supernatants were collected. The absorbance of the supernatant was read at 540 nm. The hemolysis rate was calculated using the Eq. [2] in the Appendix 1.

In vitro drug release

Drug release rates were determined using 2 different pHs to explore the pH sensitivity of the nanomedicine. ZDC@M (2 mg/mL) was dissolved in PBS solution at pH 5.5/7.4. The solution was put on a shaker at 37 ℃ for 6 h. PBS solution (500 μL) was obtained every hour and centrifuged at 12,000 rpm for 10 min. The supernatant was collected and its absorbance was acquired at 360 nm (DMDD) and 660 nm (Ce6). The new 500 μL PBS was replenished. Each group had 3 replicates. The Release rate was calculated using the Eq. [3] in the Appendix 1.

In vitro production of ROS

To detect the rate of ROS production by ZDC@M *in vitro*, 1,3-diphenylisobenzofuran (DPBF) was used. Absorbance values of the DPBF, DPBF + ZDC@M, and DPBF + ZDC@M + US groups were determined at 410 nm at 1-min intervals. The remaining DPBF rate was calculated using the Eq. [4] in the Appendix 1.

In vitro cellular uptake of nanomedicines

A total of 3×10^5 4T1 cells were seeded into a 6-well plate and incubated overnight. Then, 20 μg/mL of ZDC@M (8 μg/mL DMDD and 1.5 μg/mL Ce6) nanomedicine solutions at pH 7.4/5.5 were used to incubate cells for 4 h. After washing with PBS, treated cells were collected. Flow cytometry (BD, USA) was performed to explore the cellular uptake of nanomedicines by 4T1 cells.

The red fluorescence intensity of Ce6 inside 4T1 cells was analyzed by a LCSM.

Effect of nanomedicines on cellular ROS levels

The production of cellular ROS by nanomedicines was detected by DCFH-DA (2,7-dichlorodihydrofluorescein diacetate). A total of 3×10^5 4T1 cells were seeded into a 6-well plate, incubated overnight, and exposed to medium containing ZC, ZD, ZDC, ZDC@M, and ZDC@M+US (DMDD 8 μg/mL and Ce6 1.5 μg/mL). Cells were subjected to US at 1.0 MHz and 1.5 W/cm^2 for 3 min. Medium with DCFH-DA (5 mM) was added to the plates after 4 h and cultured for 30 min. Produced ROS were observed under a fluorescence microscope.

In vitro cytotoxicity assay

Cell cytotoxicity of nanomedicines against 4T1 cells was determined using the CCK-8 assay. The 4T1 cells were seeded into a 96-well plate and incubated for 24 h. Then, nanomedicines were added to each well and cultured for 24 h (n=5). After washing with PBS, medium (100 μL) with CCK-8 (10 μL) was added to each well. Then, 1 h later, the absorbance of each plate was read at 450 nm using a microplate reader. The absorbance was used to calculate the survival rate of 4T1 cells.

Effect of nanomedicines on cell apoptosis

The apoptosis of 4T1 cells by nanomedicines was analyzed by the Annexin V-FITC Apoptosis Detection Kit (Beyotime, China). The 4T1 cells (3×10^5/well) were seeded into a 6-well plate, incubated overnight, and exposed to the medium containing ZC, ZD, ZDC, and ZDC@M (8 μg/mL DMDD and 1.5 μg/mL Ce6). US was applied at 1.0 MHz and 1.5 W/cm^2 for 3 min. Supernatants and cells were collected

after 4 h. Then, 195 μL of binding buffer as well as 10 μL of PI and 5 μL of Annexin V-FITC were added and cultured for 20 min under dark conditions. Finally, the apoptotic rate of cells was determined by flow cytometry.

Live/dead cell detection

The Calcein/PI Live/Dead Viability/Cytotoxicity Assay Kit (Beyotime, China) was applied to stain live and dead cells. The 4T1 cells (3×10^5/well) were seeded into a 6-well plate overnight and exposed to medium containing ZC, ZD, ZDC, ZDC@M, and ZDC@M+US (DMDD 8 μg/mL and Ce6 1.5 μg/mL). US was applied at 1.0 MHz and 1.5 W/cm^2 for 3 min. Detection buffer (1 mL) as well as Calcein-AM (1 μL) and PI (1 μL) were added to the plates after 4 h. After incubation for 30 min, the fluorescence of dead and live cells was observed under a fluorescence microscope.

In vivo safety analysis

Four-week-old female nude mice were assigned to 3 groups randomly (n=3). Two of the 3 groups were administered with 200 μL of ZDC@M (7 mg/kg Ce6 and 35 mg/kg DMDD) 3 times every 3 days via the tail vein. The last group was administered with the same amount of PBS. On day 10 and day 30, nude mice were sacrificed and blood samples were collected. In addition, major organs (heart, liver, spleen, lung, and kidney) were collected and stained with hematoxylin and eosin (H&E) for histological and biochemical analysis.

In vivo anti-tumor effect of nanomedicines

Tumor-bearing nude mouse models were constructed to explore the anti-tumor effect of ZDC@M+US on tumor growth *in vivo*. The nude mice (5 weeks) were injected subcutaneously on the right front leg with 1×10^5 4T1 cells. Mice were randomly divided into 6 groups (n=5) when a tumor size of 80–100 mm^3 was obtained. Mice were injected with PBS, ZC, ZD, ZDC, and ZDC@M at doses of 7 mg/kg Ce6 and 35 mg/kg DMDD through the tail vein. The groups included the CON (PBS), ZC, ZD, ZDC, ZDC@M, and ZDC@M+US groups. Different nanomedicines were administered every 3 days for 9 days. US was performed at 1.0 MHz and 1.5 W/cm^2 for 3 min after 6 h of administration. Body weight and tumor volume were recorded every 2 days. Mice were sacrificed on day 20, tumors were collected, and H&E staining and immunohistochemistry (IHC) were performed. Tumor volume and the tumor inhibition rate (TIR) were calculated as follows:

$$Tumor\ volume\left(cm^3\right)=\left(Tumor\ length\times Tumor\ width^2\right)/2 \quad [1]$$

$$TIR\left(\%\right)=\left(V_{CON}-V\right)/V_{CON}\times100\% \quad [2]$$

Western blot assay

Total proteins were lysed and extracted using RIPA buffer with PMSF from 4T1 cells. Subsequently, protein samples were loaded onto SDS-PAGE gels for separation and transferred onto polyvinylidene fluoride (PVDF) membranes. After being incubated with blocking buffer at 37 ℃ for 30 min, the membranes were incubated overnight at 4 ℃ with primary antibodies against β-actin (1:2000, Proteintech, China), cleaved caspase-3 (1:1,000, CST, US), Bcl-2 (1:1,000, Proteintech, China), and Bax (1:2,000, CST, US). After washing thrice with TBST, the membranes were incubated with the secondary antibody at 37 ℃ for 1 h. ECL Western Blotting Substrate was applied to analyze immunoblots.

Statistical analysis

Data were subjected to descriptive statistics and single-factor analysis of variance (ANOVA). All data were shown as mean ± standard deviation (SD). Student's *t*-test was used to analyze differences between 2 groups. $P<0.05$ was considered statistically significant.

Animal

Four-week-old female nude mice were purchase from Guangxi medical university laboratory animal center. The animal experiments were approved by the Ethics Committee of the First Affiliated Hospital of Guangxi Medical University. (No. 202009018). The study followed the national standard GB/T35892-2018 published by the Ministry of Science and Technology of the People's Republic of China on the Guidance on the Handling of Laboratory Animals and the Guide to Ethical Review of Laboratory Animals-Animal Welfare. A protocol was prepared before the study without registration.

Results

Characterization of nanomedicines

The morphology and structure of nanomedicines were

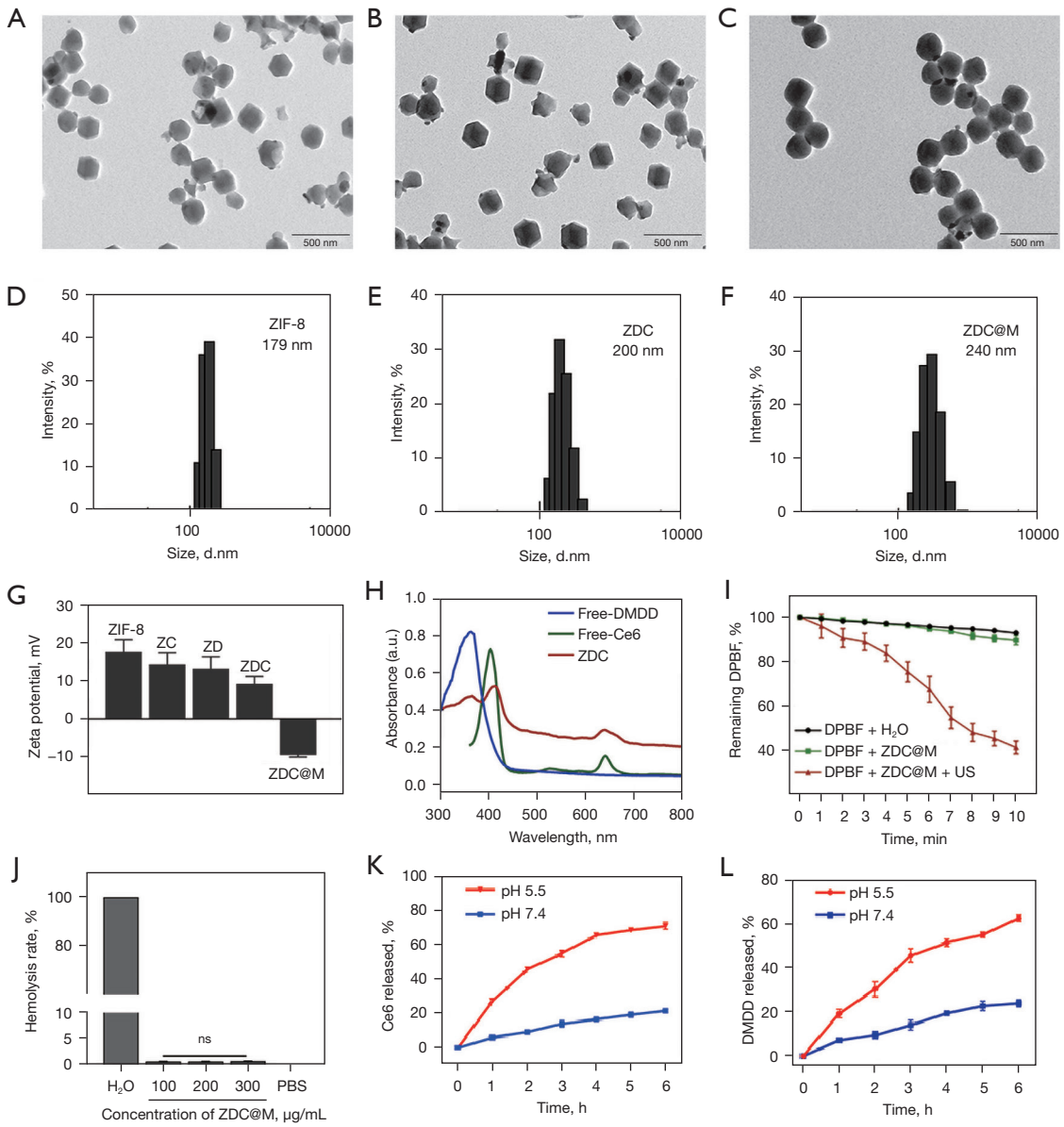

Figure 2 The morphology and structure of nanomedicines. TEM images of ZIF-8 (A), ZDC (B), and ZDC@M (C). Hydrated nanoparticle size distribution of ZIF-8 (D), ZDC (E), and ZDC@M (F). Zeta potential of different nanoparticles (G). Ultraviolet-visible absorption spectra of Ce6, DMDD, and ZDC (H). Reactive oxygen species (ROS) production by ZDC under different conditions (I). Hemolysis rate at different concentrations of the nanoparticles (J). Ce6 (K) and DMDD (L) release curves of ZDC@M triggered by different pHs. TEM, transmission electron microscopy; ZIF-8, zeolitic imidazole frameworks-8; ZDC@M, ZIF-8@ DMDD/Ce6@ cytomembrane; SDT, sonodynamic therapy; DMDD, 2-dodecyl-6-methoxycyclohexa-2,5-diene-1,4-dione; ns, no significant; PBS, phosphate buffer solution.

analyzed by TEM and SEM. ZDC@M nanomedicines were synthesized by loading DMDD and Ce6 onto ZIF-8, and then coating with the cytomembrane of 4T1 cells. DMDD and Ce6 were mainly loaded into the pores of the ZIF-8 frame, therefore, the structure and morphology of ZDC were similar with ZIF-8 (*Figure 2A*,*2B*). TEM analysis showed that ZDC@M nanomedicine was fully coated with cytomembrane (*Figure 2C*). TEM and SEM images showed that ZDC@M nanomedicine exhibited a spherical shape (*Figure 2C* and Figure S1) with a film of about 15–20 nm

on the surface, indicating successful coating with 4T1 cell membrane. The average diameters of ZIF-8, ZDC, and ZDC@M were approximately 179 nm, 200 nm, and 240 nm, respectively (*Figure 2D-2F*). Gel electrophoresis analysis demonstrated that ZDC@M had a similar protein profile to 4T1 cytomembrane, suggesting that the cytomembrane was successfully loaded (Figure S2).

The zeta potentials of ZIF-8, ZD, ZC, ZDC, and ZDC@M were 19.9, 16.5, 15.4, 7.81, and -9.18 mV, respectively (*Figure 2G*). Loading of the cytomembrane which carries a net negative charge resulted in charge reversal. The characteristic absorption spectrums of Ce6 (400 and 660 nm) and DMDD (362 nm) were observed in the spectrum of ZDC@M (*Figure 2H*). These results indicate the successful synthesis of nanocomposites. Encapsulation efficiencies of Ce6 and DMDD were 71.64%±1.41% and 50.7%±1.58%, respectively. This finding suggests that DMDD and Ce6 were effectively co-loaded onto ZIF-8 to form a combination therapy.

The results showed that the amount of unreacted DPBF in the ZDC@M+US group was significantly lower than H_2O group and ZDC@M group, indicating that US irradiation generated high ROS levels from Ce6 (*Figure 2I*).

Blood compatibility of the ZDC@M nanocomposite was assessed through the hemolysis assay. A hemolysis rate lower than 10% is safe for intravenous injection (34). Even though the concentration of ZDC@M was up to 300 μg/mL, its hemolysis rate was less than 2% (*Figure 2J* and Figure S3). This suggests that the ZDC@M nanocomposite had good blood compatibility.

Drug-releasing rates of Ce6 and DMDD from ZDC@M were explored at pH 5.5 and pH 7.4. Due to the pH-responsive characteristic, approximately 62.9% of loaded DMDD and 71.2% of loaded Ce6 were released from ZDC@M after incubation at pH 5.5 for 6 h, which were significantly higher compared with the release rate at pH 7.4 (*Figure 2K,2L*). This finding indicates that the nanomedicine was released more under an acidic environment and can be used to achieve targeted therapy.

In vitro cellular uptake and ROS generation

The distribution of Ce6 after uptake by 4T1 cells was observed under an LCSM to explore the targeting ability of ZDC@M. The results showed that the red fluorescence intensity of Ce6 in 4T1 cells cultured at pH 5.5 was stronger relative to that cultured at pH 7.4 (*Figure 3*). This is attributed to the uptake of more nanomedicines by cells under an acidic environment. In addition, the intensity of red fluorescence of Ce6 was higher in 4T1 cells cultured with ZDC@M compared with the intensity after culturing with ZDC at the same pH (*Figure 3A,3C*). This finding is attributed to the coating of ZDC with 4T1 cell membrane which enhanced the identification of nanomedicines, resulting in increased targeting ability of ZDC@M. Flow cytometry results were consistent with LCSM findings (*Figure 3B,3D*).

ROS levels after administration of nanomedicines were determined by the DCFH-DA method using LCSM. The CON, ZD, ZC, and ZDC groups showed low intensity of green fluorescence (*Figure 3E,3F*). The ZDC@M group exhibited relatively stronger intensity of green fluorescence, implying that the nanomedicines treated without US only produced low ROS levels. Cells incubated with ZDC@M+US exhibited the highest fluorescence intensity, indicating that US irradiation of Ce6 did result in the production of high ROS levels.

In vitro therapeutic effects

Cytotoxicity of the nanomedicines on 4T1 cells was analyzed to explore the therapeutic effects. The best loading content of DMDD on ZDC@M was also determined. Cell viability was inhibited below 50% when the loading level was up to 8 mg, suggesting that the initial loading amount of DMDD was 8 mg (*Figure 4*). The results showed that ZIF-8 and ZIF-8 @ cytomembrane (Z@M) exhibited negligible toxic effects towards 4T1 cells and the cell viability levels were above 90%, with probe concentrations up to 100 μg/mL (*Figure 4B*). Notably, US alone had very little killing effect towards 4T1 cells, and ZD, ZC, and ZDC exhibited low cytotoxicity (*Figure 4C*). In addition, the killing effect of nanomedicines was significantly increased with the increase in concentration of ZDC@M after US irradiation (*Figure 4C*). The cell survival rates in the ZD, ZC, ZDC, and ZDC@M groups at concentrations equivalent to 1.5 μg/mL Ce6 and 8 μg/mL DMDD were lower relative to concentrations equivalent to 0.75 μg/mL Ce6 and 4μg/mL DMDD. Cell viabilities of the ZDC groups were lower compared with the cell viabilities in the ZD and ZC groups. This indicates that the combination of the 2 drugs improved the killing effect compared with the use of a single drug. Moreover, the survival rates of 4T1 cells with ZDC@M obtained after loading the cell membrane were lower than the survival rates of the ZDC groups. This can be attributed to increased targeting

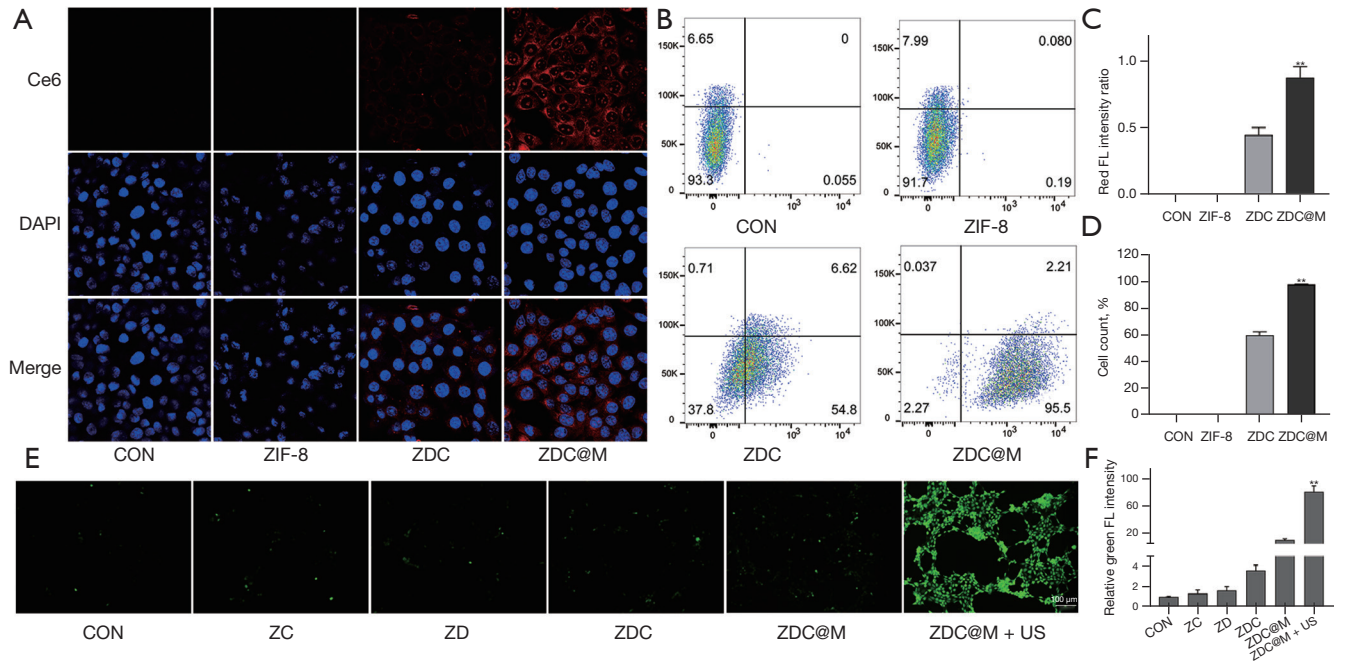

Figure 3 *In vitro* cellular uptake and ROS generation. Fluorescence imaging (600×) (A) and flow cytometry (quantitative detection of intracellular Ce6 fluorescence) (B) of 4T1 cells incubated with different nanoparticles at pH 7.4 and 5.5, respectively. ROS production was detected by fluorescence of DCFH-DA in 4T1 cells (E) (100×). Quantification of intracellular fluorescence intensity in A (C). Level of 4T1 cells with intracellular fluorescence of B (D). Quantification of intracellular fluorescence intensity in E (F). species. (A) DAPI staining. (E) Fluorescent probe DCFH-DA. **P<0.0001. ZIF-8, zeolitic imidazole frameworks-8; ZDC@M, ZIF-8@ DMDD/Ce6@ cytomembrane; ROS, reactive oxygen species.

ability of the nanomedicine resulting in uptake of high nanocomposite amounts by cells and an increase in the killing effect on cancer cells (*Figure 4C*). Furthermore, cell viability was significantly reduced to approximately 45% after treatment with US, which was similar to the cell viability without US treatment. These results indicated a good combined effect of SDT and Chinese medicine.

Co-staining of Calcein-AM (green) and PI (red) and flow cytometry analyses were conducted to explore the co-therapeutic effect of nanomedicines. The CON, ZD, ZC, ZDC, and ZDC@M groups exhibited a low intensity of red fluorescence (*Figure 4D,4F*). The US irradiated ZDC@M group presented a significantly higher intensity of red fluorescence, indicating that the therapeutic effect of the SDT and DMDD co-therapy group (ZDC@M+US) was relatively higher compared with that of the group without SDT (ZDC@M) (P<0.0001).

Flow cytometry results were consistent with the Calcein-AM/PI co-staining results (*Figure 4E,4G*). Apoptotic cell populations of the CON, ZC, ZD, ZDC, and ZDC@M groups were 13.63%, 17.71%, 20.66%, 34.71%, and 40.61%, respectively. The US irradiated ZDC@M exhibited a significantly higher proportion of apoptotic cells at 58.27% (P<0.0001). Live cells significantly decreased, accompanied by an increased number of apoptotic cells following SDT treatment, compared to the other 5 groups. These findings show that the nanomedicine had an enhanced lethal effect through the combination of DMDD and SDT on cancer cells.

In vivo biocompatibility of nanomedicines

The biocompatibility of nanoparticles was evaluated to explore their safety *in vivo*. No significant differences were observed in the counts of RBCs, white blood cells (WBCs), hemoglobin (Hb), and platelets (PLTs) among the treatment groups on day 10 and day 30 and the CON group, suggesting that ZDC@M had no blood toxicity effects *in vivo* (*Figure 5A*). In addition, no significant differences were observed in the levels of aspartate aminotransferase (AST), alanine aminotransferase (ALT), alkaline phosphatase (ALP), and blood urea nitrogen (BUN) between the treatment groups on day 10 or 30 and the CON group on day 10 and 30, indicating that the nanomedicine had no

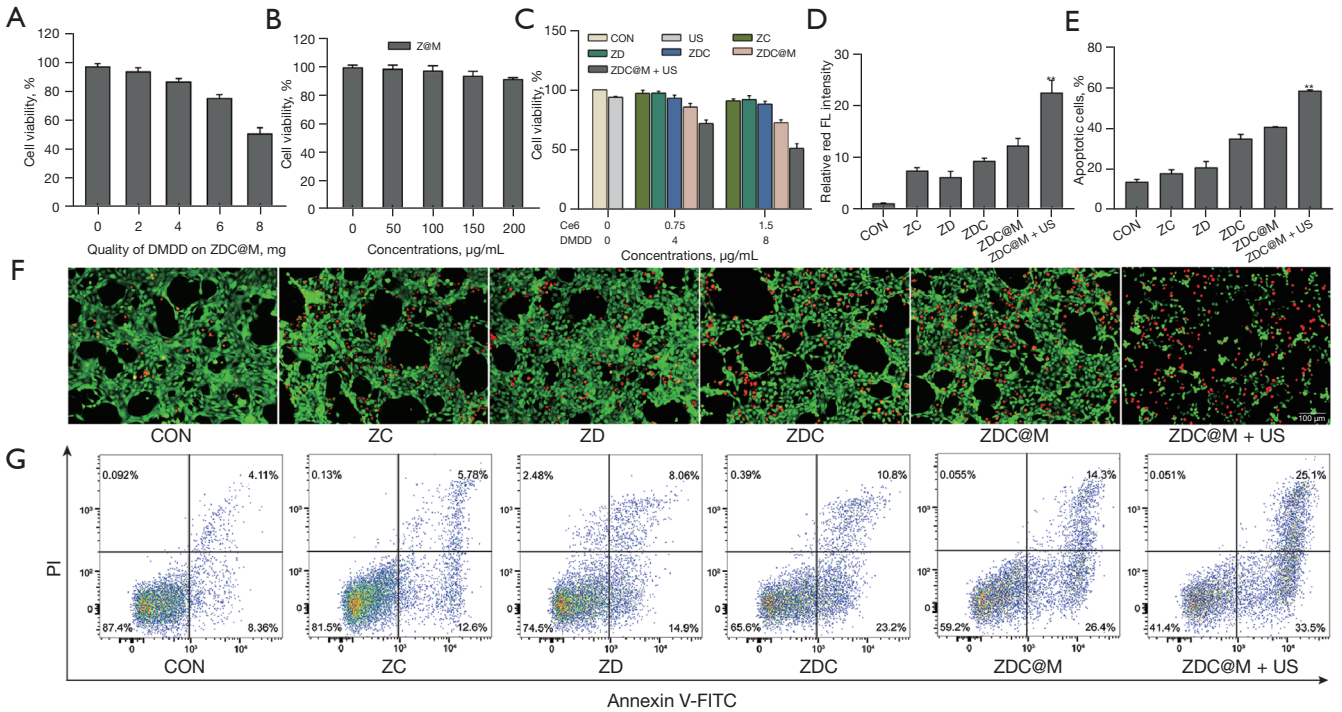

Figure 4 *In vitro* therapeutic effects of nanoparticles. Cell viabilities of 4T1 cells incubated with ZDC at different loading concentrations of DMDD (A). Cell viabilities of 4T1 cells treated with different nanomedicines (B) and (C). Quantification of intracellular fluorescence intensity (D) of Calcein-AM and PI staining fluorescence images (F). The bar chart indicates the population of apoptotic cells (E) in the flow cytometry analysis (G). **P<0.0001. ZDC, ZIF-8@ DMDD/Ce6; DMDD, 2-dodecyl-6-methoxycyclohexa-2,5-diene-1,4-dione.

hepatotoxicity and nephrotoxicity effects (*Figure 5A*).

H&E staining of major organs from nude mice administered with ZDC@M at 2 timepoints was performed to further explore histological changes induced by ZDC@M. The findings showed no obvious damage and pathological changes in the heart, liver, spleen, lungs, and kidneys of the 2 experimental groups compared with the CON group (*Figure 5B*). This finding indicates that the nanomedicine had no apparent biological toxicity *in vivo*. The results suggest that ZDC@M is a safe nanomedicine and can be used for *in vivo* treatment.

In vivo anti-tumor efficacy

A nude mouse model bearing 4T1 cells was established to explore the anti-tumor effect of the nanomedicines. The results showed that the tumor sizes of the ZDC@M+US group were smaller compared with the tumor sizes of the other groups (*Figure 6A*). Analysis showed no significant body weight losses among the 6 treatment groups, indicating that the nanomedicines had good biocompatibility (*Figure 6B*). ZDC@M treatment significantly inhibited tumor growth relative to the level of inhibition in the other 4 groups. Notably, the ZDC@M+US group exhibited significantly slower tumor growth compared with all other groups, implying that tumor growth was inhibited. These results were consistent with the results of the TIR (*Figure 6C,6D*). This can be attributed to the release of ROS from Ce6 irradiated by US, which further increased the anti-tumor effect of ZDC@M. Therefore, the most effective anti-tumor effect was achieved by the combination of SDT and DMDD.

Moreover, H&E staining showed a significantly larger necrotic tissue area in the ZDC@M+US group compared with the other groups (*Figure 6E*), demonstrating the higher efficacy obtained by the combination of SDT and DMDD.

The probable reasons for these observed effects could be explained as follows. First, the sizes of the nanomedicines were small (approximately 200 nm), making them easily pass through the cell membranes. Moreover, the coating of the nanoparticles with homologous tumor cytomembranes enhanced the targeting ability of nanomedicines by

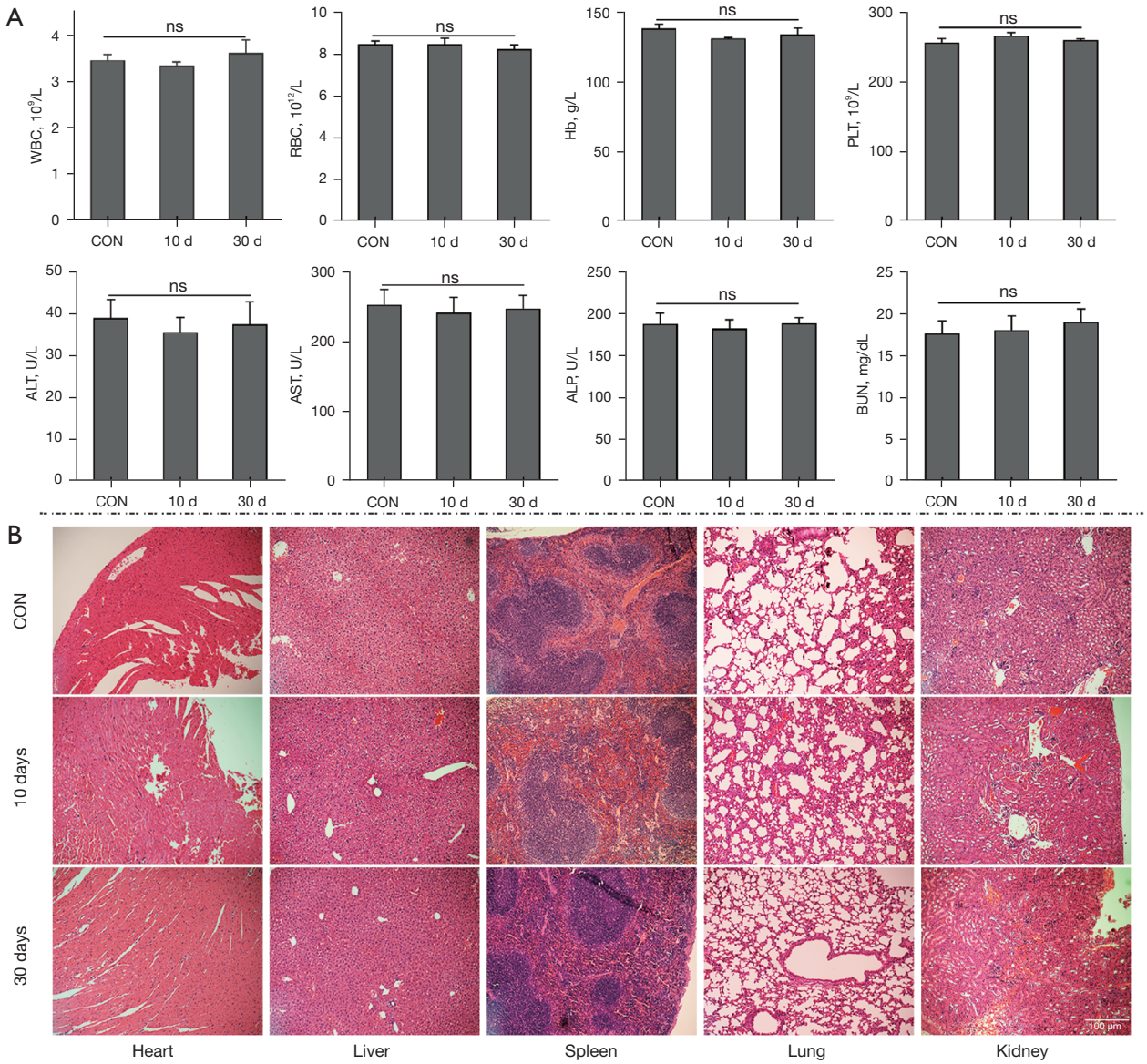

Figure 5 *In vivo* biocompatibility of nanoparticles. Changes in WBC, RBC, Hb, PLT, ALT, AST, ALP, and BUN suggesting ZDC@M had no blood toxicity effects and had no hepatotoxicity and nephrotoxicity effects *in vivo* (A). H&E staining of nude mouse organs on day 10 and day 30 after 3 injections of ZDC@M (B) (100×) showed no obvious damage and pathological changes in the heart, liver, spleen, lungs, and kidneys of the 2 experimental groups compared with the CON group. WBC, white blood cell; RBC, red blood cell; Hb, hemoglobin; PLT, platelet; ALT, alanine aminotransferase; AST, aspartate aminotransferase; ALP, alkaline phosphatase; BUN, blood urea nitrogen; ZDC@M, ZIF-8@ DMDD/Ce6@ cytomembrane; ns, no significant.

improving recognition by cells, which increases uptake by 4T1 cells. In addition, ZIF-8 was characterized by good loading capacity and pH-responsive release (35). The pH-responsive release property increases drug release in the tumor location and improves local drug concentration (36). Furthermore, ROS released by Ce6 had a synergistic effect with Chinese medicine monomer components (DMDD), thus increasing the anti-tumor efficacy.

Nanomedicine-SDT therapy induces apoptosis in 4T1 cells

Flow cytometry analysis illustrated that the nanomedicines

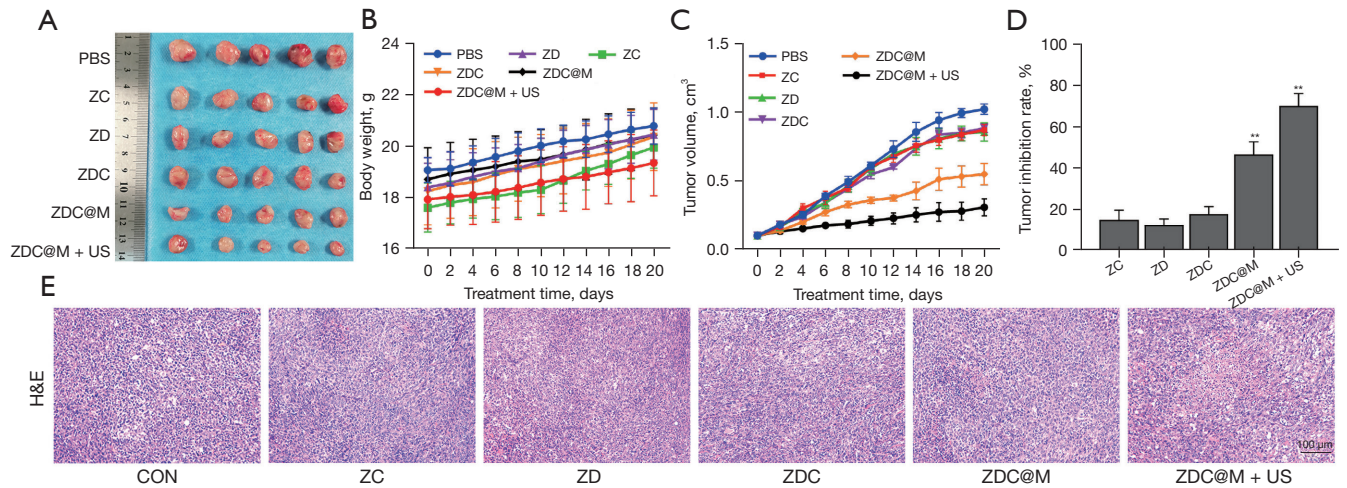

Figure 6 *In vivo* therapeutic effect of nanoparticles. Tumor size (A), body weight change (B), tumor volume change (C), and tumor inhibition rate (D) of 4T1 tumor-bearing nude mice under different treatments. H&E staining of tumor after different treatments (100×) (E). n=5. **P<0.0001.

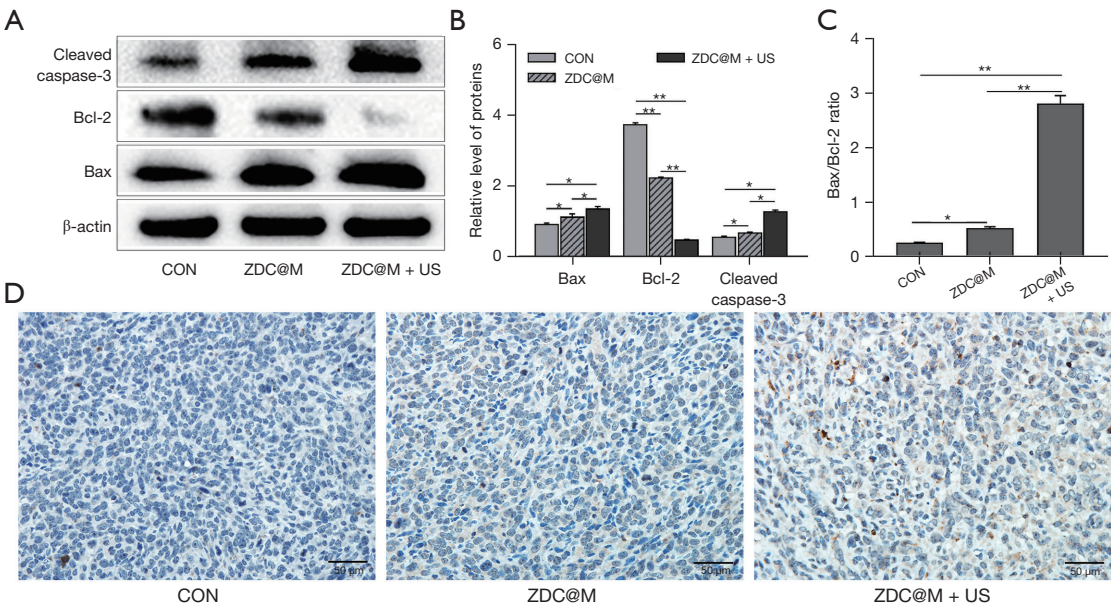

Figure 7 The ZDC@M+ ultrasound (US) induces morphological and molecular markers of apoptosis. Cleaved caspase-3, Bax, and Bcl-2 protein level (A). The bar chart indicates the relative density of cleaved caspase-3, Bax, and Bcl-2 to β-actin in A (B). The ratio of Bax/Bcl-2 (C). Immunohistochemistry staining of tumor tissues after different treatments (D). *P<0.05, **P<0.0001. ZDC@M, ZIF-8@ DMDD/Ce6@ cytomembrane.

induced cell apoptosis. Further analysis was performed to explore the expression of apoptosis-related proteins after treatment.

Bax and cleaved caspase-3 were significantly upregulated and Bcl-2 was significantly downregulated after treatment with ZDC@M compared with the expression levels in the CON group (*Figure 7A*). Notably, obvious upregulation of Bax and cleaved caspase-3 and downregulation of Bcl-2 were observed after subjecting cells to SDT compared with the levels in the CON and ZDC@M groups

(*Figure* 7*A*,7*B*) (P<0.05). The ratio of Bax/Bcl-2 of ZDC@M+US (2.80) increased compared with that in the CON and ZDC@M groups (0.24 and 0.51, respectively) (*Figure* 7*C*) (P<0.0001). Moreover, the expression of cleaved caspase-3 in the ZDC@M+US group increased significantly compared with the ratio in the CON and ZDC@M groups (*Figure* 7*B*). These findings indicate that combination therapy with SDT and DMDD significantly downregulated Bcl-2 expression and upregulated Bax and cleaved caspase-3 expression. Furthermore, the IHC results illustrated that cleaved caspase-3 expression was upregulated in the ZDC@M+US group compared with the other 2 groups (*Figure* 7*D*).

Chemotherapy drugs, hypoxia, and DNA damage caused by excess oxidative stress and ROS accumulation can cause cell apoptosis (37,38). Increased ROS production can trigger the mitochondria-caspase pathway of apoptosis (39). The findings of the present study showed that Ce6 was activated by US and released ROS. Bax, a pro-apoptotic protein, is involved in regulating the release of cytochrome C. In contrast, as an anti-apoptotic protein, Bcl-2 inhibits the release of cytochrome C. Therefore, the Bax/Bcl-2 ratio is an indicator of susceptibility of cells to apoptosis (40,41). Damage of DNA can upregulate Bax expression and downregulate Bcl-2 expression, thus increasing the Bax/Bcl-2 ratio (39,42). This can be attributed to the collapse of the inner layer of mitochondria, thereby causing the release of cytochrome C and playing a significant role in the activation of caspase-3 (43,44). Apoptosis executioner caspase-3 is an effector of apoptosis (41,45). It is an inactive dimer, but it can be activated by cleaving caspase-3 zymogen, thus transforming to the activated caspase-3 (cleaved caspase-3) (46). Cleaved caspase-3 causes DNA fragmentation by activating endonucleases, damaging nuclear proteins and the cytoskeleton, and forming apoptotic bodies, thus leading to cellular changes corresponding to apoptosis (47,48). Hence, activation of caspase-3 promotes the occurrence of apoptosis.

In our study, the Bax/Bcl-2 ratio and cleaved caspase-3 increased significantly, indicating the induction of 4T1 cells towards apoptosis. These results suggest that the co-therapy of SDT and DMDD increased the apoptosis of 4T1 cells, thus enhancing the apoptosis effect of the nanocomposites.

Discussion

Breast cancer is the most frequently diagnosed cancer in women and ranks second among causes for cancer related death in women (49). Breast cancer therapy involves a multidisciplinary approach comprising surgery, radiotherapy, neoadjuvant and adjuvant therapy (50). Despite the remarkable improvements in the outcome of these patients obtained in the last decade, we have to find more novel therapies to reduce the adverse effects of conventional therapy. DMDD has been reported to inhibit a variety of cancer cell lines. Previous study has showed DMDD can inhibit proliferation, migration, and invasion and induces apoptosis and cell-cycle arrest of 4T1 breast cancer cells. DMDD can also inhibit the growth in mice (9). Besides, SDT generates reactive oxygen species (ROS) by ultrasonic excitation to kill cancer cells (13).

We take advantage of nanomedicine to encapsulate DMDD and Ce6 into ZIF-8 framework. We also evaluate the biocompatibility and *in vivo* safety of the nanomedicine. Our experiment showed that Nanomedicine-SDT therapy have great anti-cancer effect both *in vivo* and *in vitro*. Overall, Nanomedicine-SDT therapy is a potential strategy for breast cancer

Conclusions

In summary, a pH-sensitive release ZIF-8 MOF was successfully constructed in this study by loading DMDD and Ce6, which can be used as a combination therapy of SDT and Chinese medicine. The findings showed that ZDC@M has good targeting ability and biocompatibility properties. In addition, the combination of SDT and Chinese medicine monomer components (DMDD) enhanced the anti-cancer effect of ZDC@M by inducing cell apoptosis. These results indicated that the combination of DMDD with SDT has high potential for enhancing the anti-tumor effect against BC. But there are still some limitations to be considered for SDT. Firstly, the specific mechanisms of SDT for cancer therapy are not clear and some remain controversial. Secondary, novel sonosensitizers with less phototoxic and high therapeutic efficacy have yet to be explored.

In addition, the clinical translation of nanomedicine products faces several challenges. First, biological barriers reduce the permeability of nanomedicine. Second, the clinical safety of nanomedicine is still controversial. We'd like to explore more surface modification methods in order to improve the biocompatibility and biosafety of the nanomedicine. We expect to utilize the advances in materials chemistry and nanotechnology for constructing novel nanoplatforms with simplified components and

constructions.

Acknowledgments

Funding: The study received "Medical Excellence Award". The study was funded by the Creative Research Development Grant from the First Affiliated Hospital of Guangxi Medical University; The Natural Science Foundation of Guangxi (No. 2020GXNSFBA159068) and The Science and Technology Plan Project of Qingxiu District of Nanning, Guangxi (No. 2019023).

Footnote

Reporting Checklist: The authors have completed the ARRIVE reporting checklist. Available at https://atm.amegroups.com/article/view/10.21037/atm-22-3646/rc

Data Sharing Statement: Available at https://atm.amegroups.com/article/view/10.21037/atm-22-3646/dss

Conflicts of Interest: All authors have completed the ICMJE uniform disclosure form (available at https://atm.amegroups.com/article/view/10.21037/atm-22-3646/coif). The authors have no conflicts of interest to declare.

Ethical Statement: The authors are accountable for all aspects of the work in ensuring that questions related to the accuracy or integrity of any part of the work are appropriately investigated and resolved. The animal experiments were performed in accordance with the institutional guidelines for animal care and approved by the Ethics Committee of the First Affiliated Hospital of Guangxi Medical University (No. 202009018).

References

1. Yang B, Wang F, Zheng G. Transmembrane protein TMEM119 facilitates the stemness of breast cancer cells by activating Wnt/β-catenin pathway. Bioengineered 2021;12:4856-67.
2. Li Y, Zhao X, Liu Q, et al. Bioinformatics reveal macrophages marker genes signature in breast cancer to predict prognosis. Ann Med 2021;53:1019-31.
3. Wang Y, Cheng Z, Xu J, et al. Fat mass and obesity-associated protein (FTO) mediates signal transducer and activator of transcription 3 (STAT3)-drived resistance of breast cancer to doxorubicin. Bioengineered 2021;12:1874-89.
4. Miller KD, Nogueira L, Mariotto AB, et al. Cancer treatment and survivorship statistics, 2019. CA Cancer J Clin 2019;69:363-85.
5. Jinghua H, Qinghua Z, Chenchen C, et al. MicroRNA miR-92a-3p regulates breast cancer cell proliferation and metastasis via regulating B-cell translocation gene 2 (BTG2). Bioengineered 2021;12:2033-44.
6. Sun X, Chang X, Wang Y, et al. Oroxylin A Suppresses the Cell Proliferation, Migration, and EMT via NF-κB Signaling Pathway in Human Breast Cancer Cells. Biomed Res Int 2019;2019:9241769.
7. Han S, Gao H, Chen S, et al. Procyanidin A1 Alleviates Inflammatory Response induced by LPS through NF-κB, MAPK, and Nrf2/HO-1 Pathways in RAW264.7 cells. Sci Rep 2019;9:15087.
8. Chen C, Nong Z, Xie Q, et al. 2-Dodecyl-6-methoxycyclohexa-2,5-diene-1,4-dione inhibits the growth and metastasis of breast carcinoma in mice. Sci Rep 2017;7:6704.
9. Zhou X, Wu X, Qin L, et al. Anti-Breast Cancer Effect of 2-Dodecyl-6-Methoxycyclohexa-2,5-Diene-1,4-Dione in vivo and in vitro Through MAPK Signaling Pathway. Drug Des Devel Ther 2020;14:2667-84. Erratum in: Drug Des Devel Ther 2020;14:4575-7.
10. Gao Y, Huang R, Gong Y, et al. The antidiabetic compound 2-dodecyl-6-methoxycyclohexa-2,5-diene-1,4-dione, isolated from Averrhoa carambola L., demonstrates significant antitumor potential against human breast cancer cells. Oncotarget 2015;6:24304-19.
11. Muhammed E, Chen L, Gao Y, et al. Chemo-treated 4T1 breast cancer cells radiation response measured by single and multiple cell ionization using infrared laser trap. Sci Rep 2019;9:17547.
12. Wang L, Yang X, Song Q, et al. Uncovering the Pharmacological Mechanism of 2-Dodecyl-6-Methoxycyclohexa-2,5 -Diene-1,4-Dione Against Lung Cancer Based on Network Pharmacology

and Experimental Evaluation. Front Pharmacol 2021;12:617555.
13. Pan X, Wang H, Wang S, et al. Sonodynamic therapy (SDT): a novel strategy for cancer nanotheranostics. Sci China Life Sci 2018;61:415-26.
14. Browning RJ, Able S, Ruan JL, et al. Combining sonodynamic therapy with chemoradiation for the treatment of pancreatic cancer. J Control Release 2021;337:371-7.
15. Nesbitt H, Logan K, Thomas K, et al. Sonodynamic therapy complements PD-L1 immune checkpoint inhibition in a murine model of pancreatic cancer. Cancer Lett 2021;517:88-95.
16. Bunevicius A, Pikis S, Padilla F, et al. Sonodynamic therapy for gliomas. J Neurooncol 2022;156:1-10.
17. Son S, Kim JH, Wang X, et al. Multifunctional sonosensitizers in sonodynamic cancer therapy. Chem Soc Rev 2020;49:3244-61.
18. Zhu J, Wang Y, Yang P, et al. GPC3-targeted and curcumin-loaded phospholipid microbubbles for sono-photodynamic therapy in liver cancer cells. Colloids Surf B Biointerfaces 2021;197:111358.
19. Shen Y, Ou J, Chen X, et al. An in vitro study on sonodynamic treatment of human colon cancer cells using sinoporphyrin sodium as sonosensitizer. Biomed Eng Online 2020;19:52.
20. Li Q, Lin X, Fan Y, et al. Dual-sonosensitizer loaded phase-transition nanoparticles with tumor-targeting for synergistically enhanced sonodynamic therapy. Biomater Sci 2021;9:6126-41.
21. Li Q, Liu Q, Wang P, et al. The effects of Ce6-mediated sono-photodynamic therapy on cell migration, apoptosis and autophagy in mouse mammary 4T1 cell line. Ultrasonics 2014;54:981-9.
22. Bhatta A, Krishnamoorthy G, Marimuthu N, et al. Chlorin e6 decorated doxorubicin encapsulated chitosan nanoparticles for photo-controlled cancer drug delivery. Int J Biol Macromol 2019;136:951-61.
23. Gushchina OI, Larkina EA, Nikolskaya TA, et al. Synthesis of amide derivatives of chlorin e6 and investigation of their biological activity. J Photochem Photobiol B 2015;153:76-81.
24. Zhang K, Zhang Y, Meng X, et al. Light-triggered theranostic liposomes for tumor diagnosis and combined photodynamic and hypoxia-activated prodrug therapy. Biomaterials 2018;185:301-9.
25. Liu Y, Ma K, Jiao T, et al. Water-Insoluble Photosensitizer Nanocolloids Stabilized by Supramolecular Interfacial Assembly towards Photodynamic Therapy. Sci Rep 2017;7:42978.
26. Yan L, Yang P, Cai H, et al. ZIF-8-modified Au-Ag/Si nanoporous pillar array for active capture and ultrasensitive SERS-based detection of pentachlorophenol. Anal Methods 2020;12:4064-71.
27. Ge D, Lee HK. Zeolite imidazolate frameworks 8 as sorbent and its application to sonication-assisted emulsification microextraction combined with vortex-assisted porous membrane-protected micro-solid-phase extraction for fast analysis of acidic drugs in environmental water samples. J Chromatogr A 2012;1257:19-24.
28. Sun C, Zhang JH, Yuan XF, et al. ZIF-8-Based Quasi-Solid-State Electrolyte for Lithium Batteries. ACS Appl Mater Interfaces 2019;11:46671-7.
29. Cai W, Wang J, Chu C, et al. Metal-Organic Framework-Based Stimuli-Responsive Systems for Drug Delivery. Adv Sci (Weinh) 2019;6:1801526.
30. Cheng C, Li C, Zhu X, et al. Doxorubicin-loaded Fe3O4-ZIF-8 nano-composites for hepatocellular carcinoma therapy. J Biomater Appl 2019;33:1373-81.
31. An J, Hu YG, Li C, et al. A pH/Ultrasound dual-response biomimetic nanoplatform for nitric oxide gas-sonodynamic combined therapy and repeated ultrasound for relieving hypoxia. Biomaterials 2020;230:119636.
32. Wen Q, Lin X, Liu Y, et al. Phenolic and lignan glycosides from the butanol extract of Averrhoa carambola L. root. Molecules 2012;17:12330-40.
33. Zheng N, Lin X, Wen Q, et al. Effect of 2-dodecyl-6-methoxycyclohexa-2,5-diene-1,4-dione, isolated from Averrhoa carambola L. (Oxalidaceae) roots, on advanced glycation end-product-mediated renal injury in type 2 diabetic KKAy mice. Toxicol Lett 2013;219:77-84.
34. Xu H, Yang D, Cai C, et al. Dual-responsive mPEG-PLGA-PGlu hybrid-core nanoparticles with a high drug loading to reverse the multidrug resistance of breast cancer: an in vitro and in vivo evaluation. Acta Biomater 2015;16:156-68.
35. Sun CY, Qin C, Wang XL, et al. Zeolitic Imidazolate framework-8 as efficient pH-sensitive drug delivery vehicle. Dalton Trans 2012;41:6906-9.
36. Saisyo A, Nakamura H, Fang J, et al. pH-sensitive polymeric cisplatin-ion complex with styrene-maleic acid copolymer exhibits tumor-selective drug delivery and antitumor activity as a result of the enhanced permeability and retention effect. Colloids Surf B Biointerfaces 2016;138:128-37.
37. Park HJ, Lee R, Yoo H, et al. Nonylphenol Induces

Apoptosis through ROS/JNK Signaling in a Spermatogonia Cell Line. Int J Mol Sci 2020;22:307.
38. Mortezaee K, Salehi E, Mirtavoos-Mahyari H, et al. Mechanisms of apoptosis modulation by curcumin: Implications for cancer therapy. J Cell Physiol 2019;234:12537-50.
39. Hu Z, Lv G, Li Y, et al. Enhancement of anti-tumor effects of 5-fluorouracil on hepatocellular carcinoma by low-intensity ultrasound. J Exp Clin Cancer Res 2016;35:71.
40. Bergandi L, Mungo E, Morone R, et al. Hyperglycemia Promotes Chemoresistance Through the Reduction of the Mitochondrial DNA Damage, the Bax/Bcl-2 and Bax/Bcl-XL Ratio, and the Cells in Sub-G1 Phase Due to Antitumoral Drugs Induced-Cytotoxicity in Human Colon Adenocarcinoma Cells. Front Pharmacol 2018;9:866.
41. Obeng E. Apoptosis (programmed cell death) and its signals - A review. Braz J Biol 2021;81:1133-43.
42. Karmakar I, Haldar S, Chakraborty M, et al. Regulation of apoptosis through bcl-2/bax proteins expression and DNA damage by Zanthoxylum alatum. Pharm Biol 2016;54:503-8.
43. Elumalai P, Gunadharini DN, Senthilkumar K, et al. Induction of apoptosis in human breast cancer cells by nimbolide through extrinsic and intrinsic pathway. Toxicol Lett 2012;215:131-42.
44. Abu Zeid EH, Hussein MMA, Ali H. Ascorbic acid protects male rat brain from oral potassium dichromate-induced oxdative DNA damage and apoptotic changes: the expression patterns of caspase-3, P 53, Bax, and Bcl-2 genes. Environ Sci Pollut Res Int 2018;25:13056-66.
45. Rai NK, Tripathi K, Sharma D, et al. Apoptosis: a basic physiologic process in wound healing. Int J Low Extrem Wounds 2005;4:138-44.
46. Ke H, Wang X, Zhou Z, et al. Effect of weimaining on apoptosis and Caspase-3 expression in a breast cancer mouse model. J Ethnopharmacol 2021;264:113363.
47. D'Arcy MS. Cell death: a review of the major forms of apoptosis, necrosis and autophagy. Cell Biol Int 2019;43:582-92.
48. Poon IK, Lucas CD, Rossi AG, et al. Apoptotic cell clearance: basic biology and therapeutic potential. Nat Rev Immunol 2014;14:166-80.
49. Fahad Ullah M. Breast Cancer: Current Perspectives on the Disease Status. Adv Exp Med Biol. 2019;1152:51-64.
50. Fisusi FA, Akala EO. Drug Combinations in Breast Cancer Therapy. Pharm Nanotechnol 2019;7:3-23.

(English Language Editor: C. Betlazar-Maseh)

Cite this article as: Zhao S, Chen M, Yu Z, Pham TTH, Mo S, He Y, Liang T, Cao W, Han C. Biomimetic cytomembrane-coated ZIF-8-loaded DMDD nanoparticle and sonodynamic co-therapy for cancer. Ann Transl Med 2022;10(18):971. doi: 10.21037/atm-22-3646

